



UNIVERSITÀ DEGLI STUDI DI MILANO
FACOLTÀ DI SCIENZE E TECNOLOGIE

DEDALO
Device for Enhanced Dust Analysis
with Light Obscuration sensors

- User manual v 1.0.0 -

Academic Year 2023 - 2024

Department of Physics, University of Milan (MI, Italy)

and



EuroCold Lab
European Cold Laboratory Facilities



EuroCold Lab, European Cold Laboratory Facilities
Department of Earth and Environmental Sciences, University of
Milano-Bicocca (MI, Italy)

Authors:

dr. L.Teruzzi, PhD in Physics, Astrophysics and Applied Physics
Department of Physics, University of Milan

dr. L. Cremonesi, research fellow in Physics
Department of Earth and Environmental Sciences, University of Milano-Bicocca

prof. M.A.C. Potenza, associate professor
Department of Physics, University of Milan

Acknowledgements to:

dr. Claudio Artoni, Engeneer of the EuroCold Laboratory
Department of Earth and Environmental Sciences, University of Milano-Bicocca

prof. B. Delmonte,associate professor
Department of Earth and Environmental Sciences, University of Milano-Bicocca

prof. V. Maggi, full professor
Department of Earth and Environmental Sciences, University of Milano-Bicocca

Last revised: May 1, 2024

Contents

1 General features	8
1.1 Introduction	8
1.2 The instrument	9
2 Graphical user interface (GUI)	11
2.1 Settings and default values	12
2.2 Software measurement and analysis section	16
2.3 Data analysis	20
2.3.1 Refractive index correction	20
2.3.2 The RI correction interactive panel	25
2.3.3 Aspect-ratio correction	27
3 Appendix A: Mie theory and light extinction	29
4 Appendix B: software back-end examples and requirements	32
4.1 Folder organization	32
4.2 Required packages and setup	35
Bibliografia	35

List of Figures

1.1	The Abakus Laser Sensor (left) and its relative data processing Black Box (right).	9
2.1	GUI application, written in Python3.8 programming language, designed for Abakus laser sensor. Generally, the interface is divided in two halves: on the left, some plots and histograms are shown while on the right the user can both specify the required input parameters and read the results from data analysis. Moreover, there is the possibility to perform some data analyses, investigating refractive index values different from the default one for Abakus sensor ($n = 1.58$), calibrate the instrument and visualize the noise level for each channel.	11
2.2	Example of the right side of the GUI software, regarding all the settings and the parameters required to run correctly the measurement.	12
2.3	Example of message (warning, specifically) reported in the error box. All the messages displayed here are printed in red. Here, the "Abakus running", the "Sensor alarm" and the "RAM-buffer alarm" labels are both red, since the software is not running yet.	15
2.4	Example of the 'Size (local) and time distribution' section. On the left side of the GUI interface, the particle size distribution (blue) and the temporal evolution of the number of counts (red line - yellow filling); the first one represents the number of counts as a function of the particle diameters [μm] as set by the user in the 32 Abakus channels, while in the latter they are visualized as a function of time [s]. On the right side, in the central output window the user can see for each acquisition the number of particles detected (central column) and the total number of counts since the beginning of the measure (right column). The error output window reports with a red font any warning messages arising during the software operation and for the sake of completeness the "Noise level window" reports the voltage values [mV] of the instrument measuring channels.	16
2.5	Example of the 'Size (incremental) and time distribution' section. On the left side of the GUI interface, the particle size distribution (blue) and the temporal evolution of the number of counts (red line - yellow filling); the first one represents the number of counts as a function of the particle diameters [μm] as set by the user in the 32 Abakus channels, while in the latter they are visualized as a function of time [s]. Unlike the previous situation, here the size distribution shows the incremental number of counts for each channel and not the instant measurement. On the right side, the software settings and properties of the output windows are the same as described above (see Fig.2.4).	17

2.6 Example of the 'Voltage monitor (laser diode and RAM)' section. On the left side, during a "Live" acquisition the user can see in real time the behavior of the laser diode supply voltage (blue line) and the RAM-buffer voltage (red line). In standard operative conditions, the former should be about 5300 mV while the latter around 2800 mV. If the laser diode voltage exceeds 8 V (8000 mV) or the RAM-buffer voltage gets too low an error message raises and the user should switch the Abakus laser sensor off. NOTE: this picture shows clearly what is not supposed to happen to the laser diode voltage!	18
2.7 Data correction window. Three possible solutions for correcting and calibrating Abakus measurements are reported: (1) calibration with known calibrated samples (colloidal suspension of polystyrene nanoparticles) and comparison to Mie scattering theory; (2) refractive index correction, which is of fundamental importance in order to increase Abakus measurements accuracy; (3) aspect-ratio correction, in the case of non-spherical particles.	20
2.8 General workflow of DEDALO.	21
2.9 C_{ext} curve from Mie scattering theory (blue solid line) and the smoothed version (green solid line). The LO results for calibrated 1.0 μm , 1.8 μm , 2.9 μm , 3.5 μm and 5.0 μm polystyrene spheres are shown as red circles, compared to the expected C_{ext} values (blue triangles). The LO calibration function adopted here to invert C_{ext} to d , obtained by interpolating the experimental results, is reported as a red dashed line.	22
2.10 (a) C_{ext} LUT calculated through Mie theory for refractive indices between 1.3311 and 2.6 and particle sizes in the range 0.2–20 μm . The inset (b) on the right focuses on the ranges which were most relevant for our work: refractive indices between 1.3311 and 1.6500 and particle sizes ranging from 0.2 to 10 μm . Both images are normalized to their peak value. (c) C_{ext} vs d for different refractive indices as retrieved from the LUT. Oscillations in Mie functions leading to a non-monotonic behavior occur at smaller diameters for increasing n	23
2.11 Example of the PSD conversion process. Black solid lines represent the C_{ext} curves for $n = 1.42$, $n = 1.46$ and $n = 1.56$ respectively, according to Mie theory. The red dashed curve is the LO calibration function. The red histograms are the result of unprocessed LO measurements, whereas the black and white histograms are the effective initial Gaussian PSDs. DEDALO processes the red histograms to give the correct ones.	24
2.12 Window resuming the different kind of analyses described above. The blue histogram in the upper left corner is the raw uncalibrated size distribution measured by the Abakus laser sensor; the green one, on the right, describes the calibrated size distribution starting from the considerations explained in Section ???. Finally, the red size distribution in the lower left corner is the one obtained after the inversion with the refractive index value(s) set by the user in the appropriate window. Further information on this third procedure are presented in the following. On the bottom, the time distribution of the number of counts is reported as well, so that the user can choose to consider the whole measurement or just a slice of it (limiting consequently the number of particles visualized in the size distributions) by moving the vertical cursors.	25
2.13	26

3.1	Trend of $S(0)$ for an aqueous suspension spherical particles with different refractive indices, as a function of particles diameter between 0.1 and 10 μm	30
3.2	Trend of C_{ext} for an aqueous suspension spherical particles with different refractive indices, as a function of particles diameter between 0.1 and 10 μm	31
4.1	Abakus GUI software repository. The main script is the ‘abakus.pyw’ (the first one), while the others are classes or supplementary modules useful for the software working correctly. Some subfolders are also listed containing text files and GUI configuration files.	32

Chapter 1

General features

1.1 Introduction

Light obscuration is one of the most reliable methods for measuring the size distribution (PSD) and number concentration of sub-visible particles suspended in a liquid [1]. It is also the European Union reference for sizing, according to the ISO21501-3 standard [2]. The liquid suspension is driven through a small cell transilluminated by a laser beam. When a microparticle intercepts the beam, a photodiode detects the corresponding attenuation, thus measuring the optical extinction cross-section, C_{ext} . According to general light scattering laws, C_{ext} is mainly affected by particle size [3, 4], therefore, it is retrieved with relative ease if the refractive index is established first. Instruments based on this working principle are often called Light Obscuration (LO) sensors. They are able to characterize a wide range of particles, as small as $0.2 \mu\text{m}$ in diameter. Additionally, they are fast, easy to use, and can be used *in situ* or with minimal sample preparation. Therefore, they are suitable for real-time monitoring and process control applications [5, 6]. They provide results within seconds, which is crucial for industrial use, including pharmaceuticals and electronics applications.

The main drawback of instruments providing such mono-parametric measurements is that the refractive index cannot usually be inferred from the light scattering data. In fact, it is customary to assume a one-fits-all value, n_0 , which might differ from that of the actual particles under study; no absorption is considered. The standard calibration procedure is usually based on light scattering by polystyrene spheres: it is assumed that the size of a particle is that of the polystyrene sphere that causes the measured attenuation of the laser beam. However, the refractive index n of particles that populate real samples can appreciably differ from the reference value n_0 and can depend on temperature [7, 8] and pressure [9]. Generally speaking, particles with a larger refractive index extinguish more light than particles with a lower refractive index of the same size. This implies that the size of particles characterized by $n < n_0$ will be underestimated and vice versa [10]. Moreover, the larger the refractive index deviation from the calibration standard, the less accurate the PSD results are [11]. A larger difference in the refractive index from that of the surrounding medium accentuates this effect [11], some examples being air bubbles in water or oil droplets in water.

Other particle sizing techniques such as dynamic light scattering (DLS), laser diffraction, or Small Angle Light Scattering (LALS) may be used as complementary methods to provide additional information on particle size distribution [12, 13], at the cost of reducing the effectiveness in terms of data throughput. In some cases, the refractive index can be measured or inferred independently [14].

Here we present a ready-to-use software to overcome the limitation of having to fix the refractive index a priori. An open-source Python-based GUI code allows the user to operate an in-line LO instrument and retrieve in real-time the correct PSDs. The algorithm operates on LO data with the refractive index as a free parameter to be set according to the sample composition. The code is named DEDALO (*Device for Enhanced Dust Analyses with Light Obscuration sensors*).

We validate the method with a range of laboratory-prepared oil emulsions characterized by different refractive index values, ranging from 1.46 to 1.64. Samples have then been analyzed through a Continuous Flow Analysis (CFA) system with a commercial LO device (Abakus particle counter, Klotz GmbH, Germany).

This study builds on a collaboration between the Instrumental Optics Laboratory of the University of Milan and the EuroCold laboratory of the glaciology and palaeoclimate group at the University of Milan-Bicocca, where all these methods are adopted for characterizing micron-sized dust from ice cores. After validating our code extensively, we performed high-resolution and high throughput measurements of mineral dust in meltwater from cryosphere samples collected on an Alpine glacier currently under study by our group. Beyond the specific application discussed in this work, we believe that the applications of DEDALO could be far more general, ranging from pharmaceuticals to water quality assessments and clinical assays.

1.2 The instrument

The Abakus is a generic, engineered laser sensor produced by Klotz, Ltd. for measuring the number and size of particles in liquids and very viscous media. The measuring system is suitable for stationary lab use as well as for mobile use. By default, the device is delivered with a sensor LDS 30/30 for water and sensor LDS 45/50 for oil (additional sensors see table). The areas of application include cleanliness control of drinking water, of chemical and pharmaceutical solutions, testing of filtration facilities and checking of viscous liquids and hydraulic oils.

In Fig.(1.1) the two main components of the Abakus laser sensor in EuroCold Lab are shown.

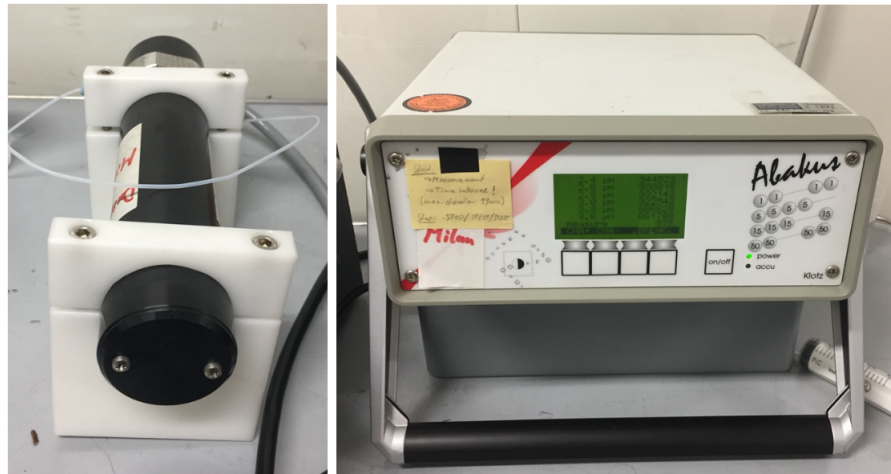


Figure 1.1: The Abakus Laser Sensor (left) and its relative data processing Black Box (right).

The instrument is made up by two parts, a detection cell and a case for data processing - as the output data visualized on the LCD screen are not the voltages recorded by the detector, but number of counts of particles with extinction diameter (d_{ext}) greater than a given value. To make an example, if the bin $2.4 \mu\text{m}$ reports N counts, it means that N particles with $d_{ext} \geq 2.4 \mu\text{m}$

were counted during the run.

While operating, the sample is pumped in the cell ¹, where a laser beam ($\lambda = 670$ nm) illuminates a photodiode sensor. Obviously, the presence of a particle would result in a negative peak in the transmitted power: this is counted in one of 32 possible bins (corresponding to 32 freely definable size classes), depending on its amplitude. This is why, if we want to produce a dimensional spectra, we absolutely need an accurate calibration (which is not straightforward, as the weight of the two contributions to extinction varies non-trivially depending on the dimensions of the particle).

Technical Specifications

Display and control	background-lighted graphical LCD display, 6-key-operation
Measuring mode	single or continuous measurement with a cycle period of 1 – 99 min
Data contents	date, time, sample number, 32 freely programmable particle size channels
Representation	cumulative and distributive particle number, volume percent distribution, conversion in the standards USP 23, ISO 4406, NAS 1638
Alarm level	for particle number, programmable for ISO or NAS classes
Printer	thermal printer DPU 414
Computer interface	RS 232 C (V. 24)
Power supply	230/115 VAC, 50/60 Hz, max. 10 W

Table 1.1: Technical data and specification about the Abakus particle counter.

Since at present there is no available official software from Klotz for data acquisition and for the subsequent analysis, an *ad hoc* Python3.9 program has been written as described in the following sections.

¹The diameter of the cell is typical for the sensor, so we will have to access it using a suitable pipe.

Chapter 2

Graphical user interface (GUI)

In order to make the software user-friendly and easily accessible, a suitable GUI interface was built in parallel. Fig.(2.1) shows what the starting interface looks like.

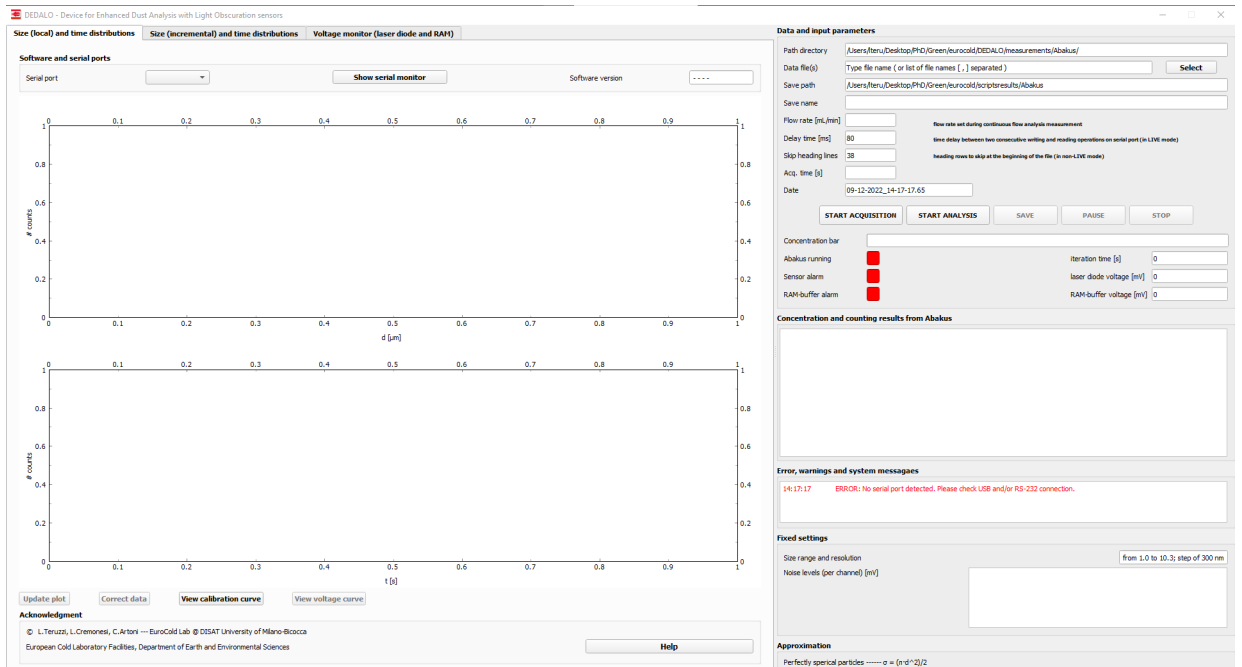


Figure 2.1: GUI application, written in Python3.8 programming language, designed for Abakus laser sensor. Generally, the interface is divided in two halves: on the left, some plots and histograms are shown while on the right the user can both specify the required input parameters and read the results from data analysis. Moreover, there is the possibility to perform some data analyses, investigating refractive index values different from the default one for Abakus sensor ($n = 1.58$), calibrate the instrument and visualize the noise level for each channel.

2.1 Settings and default values

In the following, each element in the right GUI interface is described.

Data and input parameters

Path directory	<input type="text" value="/Users/lteru/Desktop/PhD/Green/eurocold/DEDALO/measurements/Abakus/"/>	
Data file(s)	<input type="text" value="Type file name (or list of file names [,] separated)"/>	<input type="button" value="Select"/>
Save path	<input type="text" value="/Users/lteru/Desktop/PhD/Green/eurocold/scriptsresults/Abakus"/>	
Save name	<input type="text"/>	
Flow rate [mL/min]	<input type="text"/>	flow rate set during continuous flow analysis measurement
Delay time [ms]	<input type="text" value="80"/>	time delay between two consecutive writing and reading operations on serial port (in LIVE mode)
Skip heading lines	<input type="text" value="38"/>	heading rows to skip at the beginning of the file (in non-LIVE mode)
Acq. time [s]	<input type="text"/>	
Date	<input type="text" value="09-12-2022_15-12-07.24"/>	

Concentration bar	<input type="text"/>		
Abakus running	<input type="button" value=""/>	iteration time [s]	<input type="text" value="0"/>
Sensor alarm	<input type="button" value=""/>	laser diode voltage [mV]	<input type="text" value="0"/>
RAM-buffer alarm	<input type="button" value=""/>	RAM-buffer voltage [mV]	<input type="text" value="0"/>

Concentration and counting results from Abakus

Error, warnings and system messages

Fixed settings

Size range and resolution	<input type="text" value="from 1.0 to 10.3; step of 300 nm"/>
Noise levels (per channel) [mV]	<input type="text"/>

Approximation

Perfectly spherical particles ----- $\sigma = (\pi \cdot d^2)/2$

Figure 2.2: Example of the right side of the GUI software, regarding all the settings and the parameters required to run correctly the measurement.

- Data and input parameters

- Path directory: path were the files (.txt, .dat) containing full data from Abakus laser sensor, as read via serial port RS-232, are stored.
- Data file(s): file(s) name the user wants to analyze; this input can consist of both a single name and a list of names, separated by a comma (" , "). The histogram in the first left panel is always referred to the first file specified in the list, while for a comparison of all the input files the user can switch to the third panel where their normalized¹ histograms are shown.
- Save path: path were the result files (.txt, .dat) are saved.
- Save name: name specified by the user (WITH .txt or .dat extension) for saving.
- Flow rate: measured in mL/min, it is the flow rate set on the peristaltic pump during the CFA measurement.
- Skip heading lines: number of heading rows to skip before performing the analysis. These lines consist of a series of information concerning the measurement previously performed with the Abakus laser sensor (Date and time of the acquisition, software version, noise levels and so on).
- Acquisition time: measured in seconds, it is the specific period the user wants to analyze.
- Date: date and time of the measurement, saved also in the heading lines of the file.
- Buttons:
 - * START ACQUISITION: this button allows to switch between two different operating modes of the software: if "Live" is OFF, when the "Run" button is selected the GUI application reads all the input parameter previously defined and performs the analysis of a pre-recorded data file. On the contrary, if the "Live" button is ON the software performs a real time analysis during the continuous flow measurement. In the following image you can see the initial output stating which commands have been sent to the instrument and what it is doing.

Time	# counts	# counts (incremental)
18:12:05	12.0 pt	12.0 pt

- * START ANALYSIS: this button starts the (serial reading and) analysis according to the option selected by "Live".

¹The aim of such a normalization is only to make the histograms correctly comparable at sight, dividing each column by the total number of countings.

- * SAVE: this button allows the user to save all the results, also shown in the "Concentration and counting results from Abakus" output window, on a .txt file; the path to the correct directory and the file name are the ones specified before.
- * STOP: this button stops the measurement and disconnects the Abakus laser sensor.
- * PAUSE: this button stops temporarily the Abakus measurement; when pressed again, the measurement restarts.
- Concentration bar: status bar which reports the sample particle concentration as a percentage of the maximum concentration detectable by the instrument.
- Abakus running: check if the instrument is working properly by changing its color from red to green; if a problem of any kind is detected, the label becomes red again.
 - * iteration time: measured in milliseconds, it measures in real time the gap between two consecutive serial readings.
- Sensor alarm: check if the laser voltage is being measured correctly by changing its color from red to green; if any problem is detected or if the regulating voltage exceeds 7000 mV, the label becomes red again.
 - * laser diode voltage: measured in mV, it is the regulation voltage of the laser diode inside the instrument; it is a very important parameter, since if the voltage exceeds 8000 mV, the sensor must be switched off immediately and cleaned up.
- RAM buffer alarm: check if the RAM buffer voltage is being measured correctly by changing its color from red to green; if any problem is detected or if the voltage is lower than 2800 mV, the label becomes red again.
 - * RAM buffer voltage: measured in mV; as the laser diode regulating voltage, it is a very important parameter since if it becomes lower than 2800 mV, the sensor must be switched off immediately and cleaned up.
- **Concentration and counting results from Abakus**: during a LIVE measurement, in this output window are visualized the number of particles detected by the sensor each second and the total incremental number pf counts since the beginning of the measurement. On the other hand, if the software is running in non-LIVE operating mode, results are shown concerning the total number of particles detected by the Abakus, the total particle concentration and the partial concentrations for each channel as well.

```
Concentration and counting results from Abakus
09-08-2022/EDB_T5_14-52-14.txt found in directory
#####
FILE: '09-08-2022/EDB_T5_14-52-14.txt'
#####

1. Average laser diode voltage: 5323,4 mV
Avergae RAM-buffer voltage: 2873,0 mV

2. Flow rate: 2.0 mL/min
Particles detected: 2.00e+07 pt
Total particles concentration: 1.25e+06 pt/mL
Counts distribution peaked @: 1.00 ± 0.30 µm
Counts distribution average: 1.59 ± 0.18 µm
Counts distribution averaqe (arithmetical): 5.50 ± 0.05 µm
```

- **Error, warnings and system messages:** in this output window are visualized warnings and/or error messages occurred during the software running.

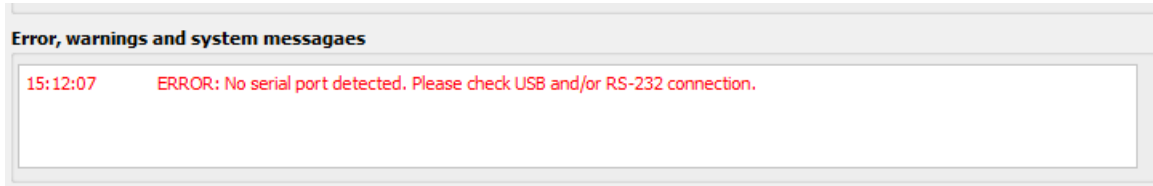


Figure 2.3: Example of message (warning, specifically) reported in the error box. All the messages displayed here are printed in red. Here, the "Abakus running", the "Sensor alarm" and the "RAM-buffer alarm" labels are both red, since the software is not running yet.

- **Fixed settings**

- Software version: kind of software originally supported by the Abakus laser sensor.
- Size range: diameter range the instrument can measure, from 1.0 up to 10.3 μm .
- Resolution: the difference in diameter that the Abakus laser sensor can resolve; in our case, it is equal to 300 nm.
- Noise levels (for each channel): noise levels measured by the Abakus laser sensor itself before the measurement starts.

- **Approximation:** simply here is specified that the Abakus sensor work in spherical approximation; this allows to derive a straightforward relation between the extinction cross-section (which is the physical parameter properly measured by the Abakus laser sensor) and the extinction diameter of the equivalent sphere:

$$\sigma_{ext} = \pi \cdot \left(\frac{d_{ext}}{2} \right)^2$$

2.2 Software measurement and analysis section

On the left GUI interface the user can firstly find four different sections that can be selected by the corresponding button on top:

- **Size (local) and time distribution:** the panel shows two kind of plots: in the upper part the particle size distribution (blue) and in the lower one the temporal evolution of the number of counts (red line - yellow filling). If the "Live" button is pressed, both the size distribution histogram and the time evolution plot are automatically update from time to time each second: the former shows the instant number of counts detected and the latter one is incremented consequently. On the other hand, if the "Live" button is off, the time plot shows the entire temporal evolution during the measurement and by clicking on it the upper size distribution is updated to the number of particles detected at that instant.

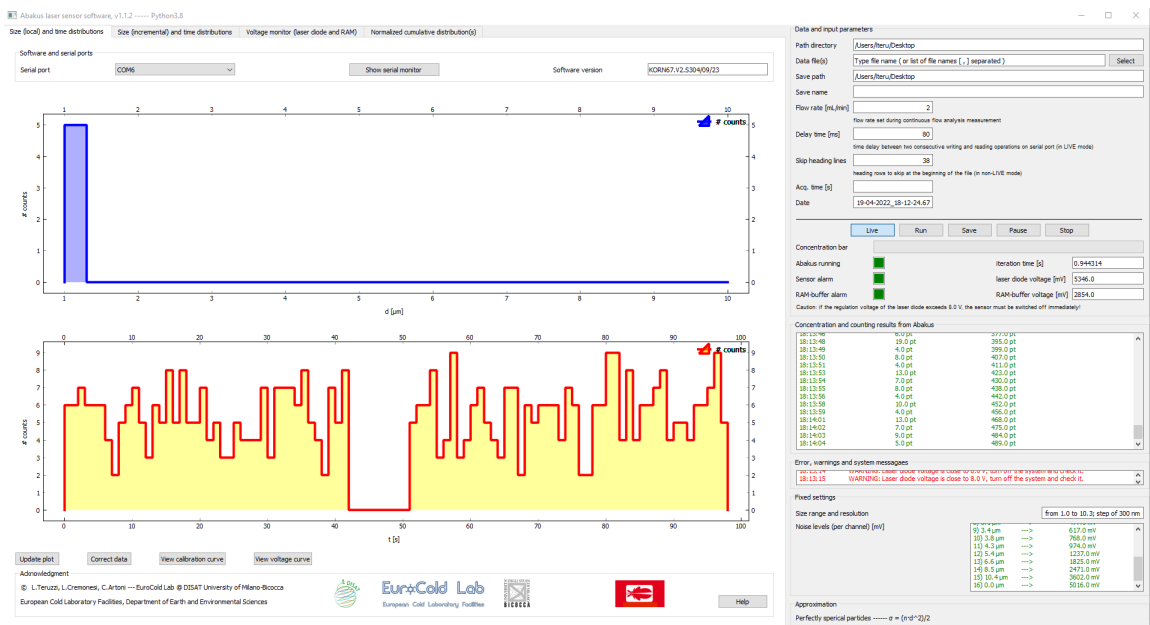


Figure 2.4: Example of the 'Size (local) and time distribution' section. On the left side of the GUI interface, the particle size distribution (blue) and the temporal evolution of the number of counts (red line - yellow filling); the first one represents the number of counts as a function of the particle diameters [μm] as set by the user in the 32 Abakus channels, while in the latter they are visualized as a function of time [s]. On the right side, in the central output window the user can see for each acquisition the number of particles detected (central column) and the total number of counts since the beginning of the measure (right column). The error output window reports with a red font any warning messages arising during the software operation and for the sake of completeness the "Noise level window" reports the voltage values [mV] of the instrument measuring channels.

- **Size (incremental) and time distribution:** as for the previous one, this panel shows two kind of plots: in the upper part the incremental particle size distribution (blue) and in the lower one the temporal evolution of the number of counts (red line - yellow filling). If the "Live" button is pressed, both the size distribution histogram and the time evolution plot are automatically update from time to time each second: the former shows the incremental

number of counts detected by the instrument and the latter one is incremented consequently. On the other hand, if the "Live" button is off, the time plot shows the entire temporal evolution during the measurement and by clicking on it the upper size distribution is updated to the total number of particles detected until then (note: not the instant number of counts but the incremental one!).



Figure 2.5: Example of the 'Size (incremental) and time distribution' section. On the left side of the GUI interface, the particle size distribution (blue) and the temporal evolution of the number of counts (red line - yellow filling); the first one represents the number of counts as a function of the particle diameters [μm] as set by the user in the 32 Abakus channels, while in the latter they are visualized as a function of time [s]. Unlike the previous situation, here the size distribution shows the incremental number of counts for each channel and not the instant measurement. On the right side, the software settings and properties of the output windows are the same as described above (see Fig.2.4).

- **Voltage monitor (laser diode and RAM):** the panel shows the behavior of both the laser (red line) and the RAM-buffer voltages (blue line) throughout the measurement. As stated previously, the laser supply voltage should stay below 8000 mV and the RAM-buffer one should be not lower than 2800 mV.²

²Sometimes it happens that for just one second the former or the latter voltage value "explodes" (that is, it becomes very large) and during the next acquisition it gets back to the default value: don't worry, it may be some kind of serial communication error and a red warning message should be visualized in the corresponding box. If the over-voltage persists, that is a problem.

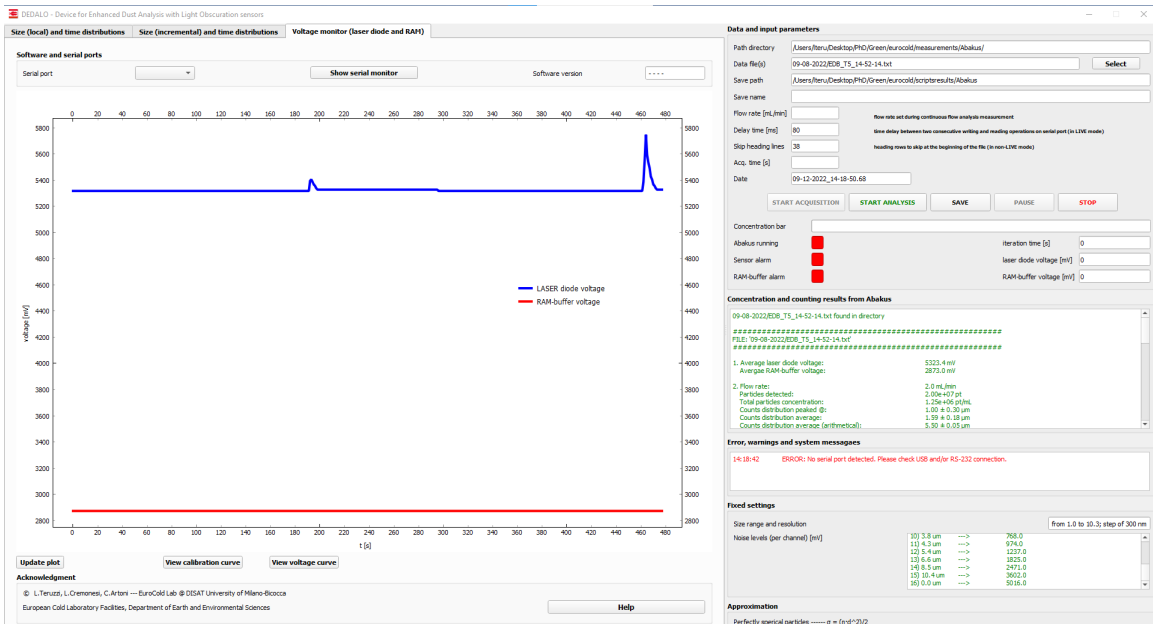


Figure 2.6: Example of the 'Voltage monitor (laser diode and RAM)' section. On the left side, during a "Live" acquisition the user can see in real time the behavior of the laser diode supply voltage (blue line) and the RAM-buffer voltage (red line). In standard operative conditions, the former should be about 5300 mV while the latter around 2800 mV. If the laser diode voltage exceeds 8 V (8000 mV) or the RAM-buffer voltage gets too low an error message raises and the user should switch the Abakus laser sensor off. NOTE: this picture shows clearly what is not supposed to happen to the laser diode voltage!

Apart from the graphic rendering, some further and useful options are available. Starting from the top:

- Serial monitor: this button opens a serial terminal in order to monitor the serial communication between the user laptop/PC and the instrument. By default, when opened this monitor acts as an output monitor: when the measurement is running, each second the Abakus serial answer is visualized as a Python bytestring. At the same time, if needed the user can also send serial command (according to the instrument protocol) and check the corresponding output.
- Update plot: the user can choose to select only a portion of the size distribution and the current plot (Size (local) and time distribution or Size (incremental) and time distribution) is updated consequently. The selected section is highlighted with a different color (red) and some statistical information on the distribution itself are visualized on a separate window: among them, for example, mean and median values, the diameter corresponding to the peak of the size distribution. This button can be pressed multiple times and the plot is always updated to the last desired portion.
- Correct data: the user can press this button if it is required to perform some deeper analyses on the size distribution directly measured by the Abakus particle counter, such as correction with the appropriate calibration curve or the fit with different refractive indices values. These procedures are better described in the following section.
- View calibration curve: the instrumental calibration curve is visualized. This curve was retrieved by measuring some well known and calibrated samples, composed of colloidal suspensions of polystyrene spheres with fixed diameters³, and checking their deviation from the Mie scattering theory prevision. As stated above, the definition of this calibration function and its importance are better presented in the following.
This button can be pressed both in "Live" and in non "Live" operating mode.
- View voltage curve: the 32 Abakus channel voltages are visualized, no more and no less. This button can be pressed both in "Live" and in non "Live" operating mode.
- Help: simply, this PDF manual is visualized.

³The polystyrene samples available in the laboratory were 1.0, 1.5, 2.1, 2.9, 3.78, 5.0 and 5.45 μm in diameter.

2.3 Data analysis

By clicking the "Correct data" button, a small interactive window is visualized so that the user can select which kind of analysis to perform, as represented in Fig.(2.7). Three main options are available, even though only two of them (#1 and #2) are well implemented and currently working and are presented in the following.

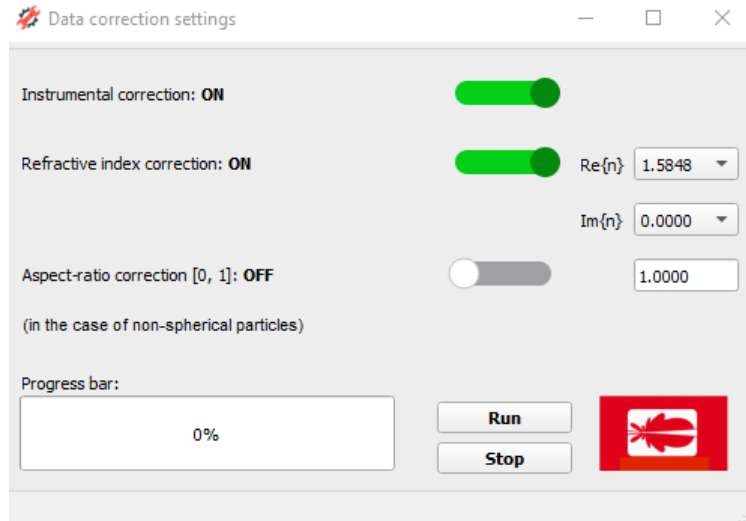


Figure 2.7: Data correction window. Three possible solutions for correcting and calibrating Abakus measurements are reported: (1) calibration with known calibrated samples (colloidal suspension of polystyrene nanoparticles) and comparison to Mie scattering theory; (2) refractive index correction, which is of fundamental importance in order to increase Abakus measurements accuracy; (3) aspect-ratio correction, in the case of non-spherical particles.

After the "Run" button is pressed, the progress bar reports the computation and analysis status.



2.3.1 Refractive index correction

DEDALO is an open-source Python-based GUI software that allows to operate an in-line LO instrument and further analyze the data by compensating for the refractive index according to the sample composition. In addition, DEDALO recovers the numeric concentration of the sample, which is not provided by the instrument. The algorithm computes C_{ext} analytically with Mie scattering theory [4, 3]; smoothing functions are then used (see below) as customary in traditional instruments. The general workflow is sketched in Figure 2.8 and can be summarized as follows:

- i) the instrumental calibration curve is retrieved by measuring mono-disperse suspensions of polystyrene spheres;
- ii) the sample PSD is measured;

- iii) each bin of the measured PSD is converted into its corresponding C_{ext} bin by computing their limits with the calibration curve, thus obtaining a new histogram by counting the number of detected particles within each C_{ext} bin;
- iv) the lower and upper limits of the C_{ext} bins are converted into the corresponding diameters through Mie theory with the new refractive index; in order to save computational resources a pre-computed look-up table is used;
- v) the corrected PSD is written on files (both spreadsheet and text file), together with some statistical markers such as the PSD mode diameter and the distribution quantiles.

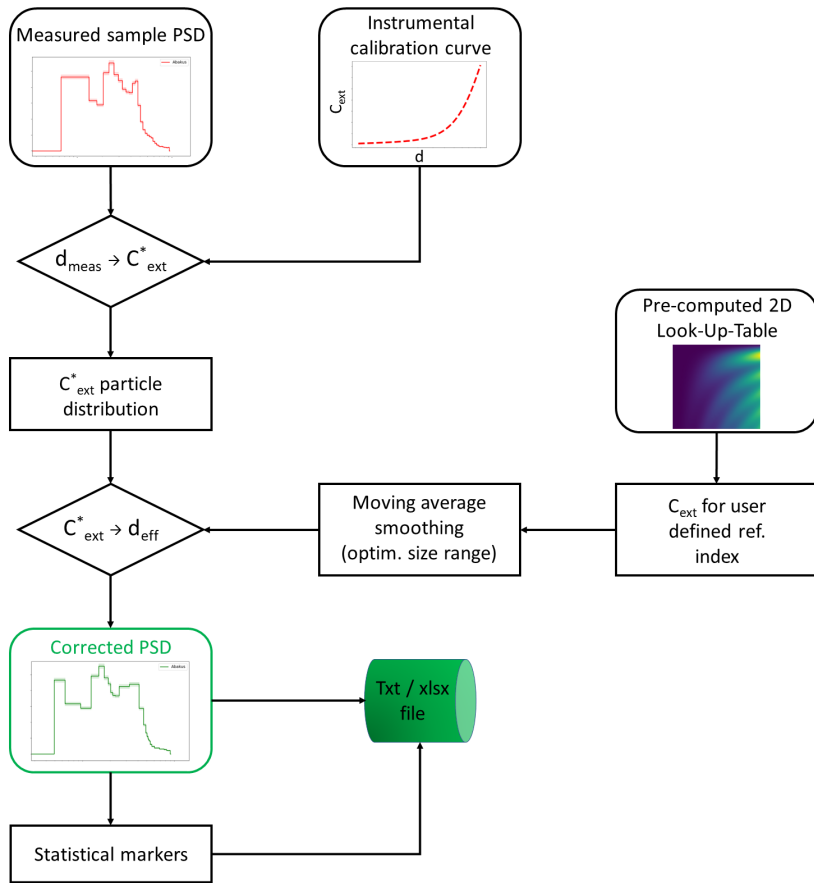


Figure 2.8: General workflow of DEDALO.

Commercial LO instruments do not typically allow the user to access raw data. A histogram of the particle counts within a given size bin is generated by inverting C_{ext} data for each particle through a calibration curve obtained from the Mie function $C_{\text{ext}} vs d$, as discussed for example in [15]. It is convenient to set the instrument in such a way that the width of the bins is uniform throughout the size range. We set the bin width to 300 nm. The calibration curve can be estimated by means of several measurements performed with mono-disperse polystyrene spheres. In Figure 2.9, we report on the (C_{ext}, d) plane the experimental results of LO measurements (red circles) for 1.0 μm , 1.8 μm , 2.9 μm , 3.5 μm and 5.0 μm calibrated polystyrene spheres and the corresponding expected positions (blue triangles). For each nominal diameter, C_{ext} was computed through Mie theory and compared to the particle size reported by the LO instrument. The Mie curve is also

reported with a blue solid line, while the green one represents a smoothed Mie curve. The LO calibration curve (red dashed line) has been obtained as a fourth-degree polynomial interpolation of the LO data in this plane:

$$C(d) = a_0 + a_1 d + a_2 d^2 + a_3 d^3 + a_4 d^4 \quad , \quad (2.1)$$

where d is the particle diameter in μm and C is in μm^2 ; the degree of the interpolating polynomial, limited by the number of available data points, is the smallest that maximizes compatibility with the real curve. Polynomial coefficients are listed in Table 2.1. We stress that the calibration curve does depend on the specific instrument or calibration, so that it must be characterized by measuring calibrated spheres, as discussed above. This step is preliminary to any further operation to recover the C_{ext} values corresponding to the diameters limiting the bins of the histogram provided by the instrument.

Table 2.1: Polynomial coefficients of the LO calibration function.

a_0 μm^2	a_1 μm	a_2 dimensionless	a_3 μm^{-1}	a_4 μm^{-2}
$-4.75 \cdot 10^{-2}$	+1.02	-4.76	$+1.21 \cdot 10^{-2}$	-6.13

As a first step, DEDALO converts the lower and upper limits of each size bin into the C_{ext} values retrieved through the calibration curve (red dashed). Then, a histogram is obtained by counting the number of detected particles within each C_{ext} bin.

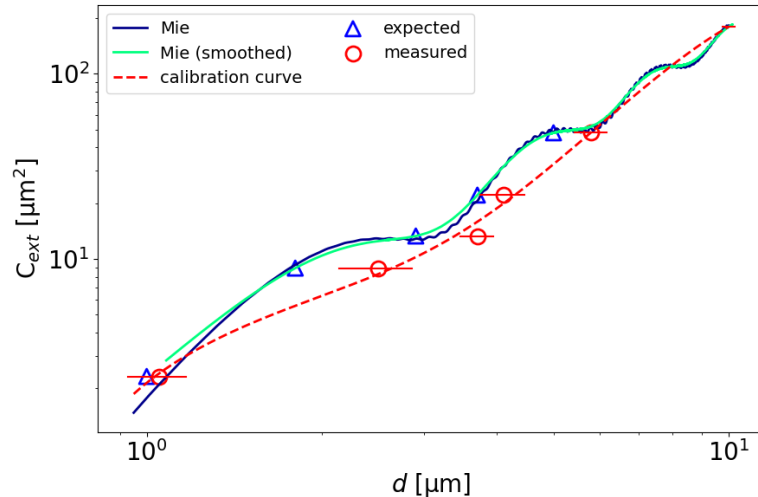


Figure 2.9: C_{ext} curve from Mie scattering theory (blue solid line) and the smoothed version (green solid line). The LO results for calibrated 1.0 μm , 1.8 μm , 2.9 μm , 3.5 μm and 5.0 μm polystyrene spheres are shown as red circles, compared to the expected C_{ext} values (blue triangles). The LO calibration function adopted here to invert C_{ext} to d , obtained by interpolating the experimental results, is reported as a red dashed line.

Finally, the limits of the C_{ext} bins are converted again into the corresponding diameters using Mie theory with a refractive index n that best suits the sample under consideration and the histogram values are divided by the corresponding bin width. We introduce a smoothing procedure to damp

any local non-monotonic behavior of the Mie functions C_{ext} vs d with a moving-average within a size range $0.1 \mu\text{m}$ wide. DEDALO dynamically adjusts the size range of the moving average depending on the desired refractive index. In Figure 2.9, the smoothed function for polystyrene is reported in green.

The core of the DEDALO algorithm is a pre-computed (C_{ext}, d) look-up table (LUT, Figure 2.10a-b) obtained by varying particle diameter and refractive index and calculating the C_{ext} values through Mie theory. The use of the LUT instead of recomputing Mie functions saves a considerable amount of computational time.

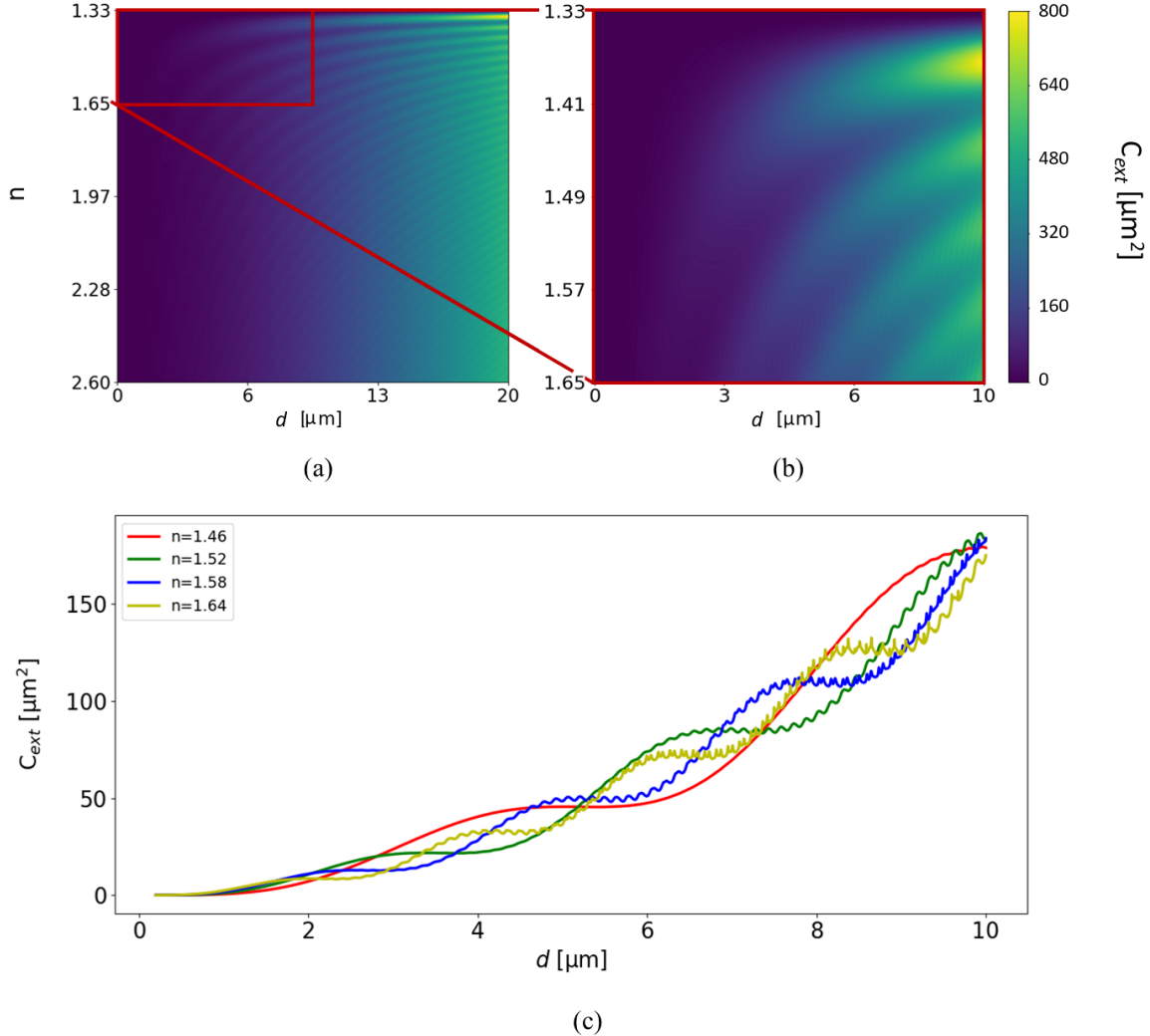


Figure 2.10: (a) C_{ext} LUT calculated through Mie theory for refractive indices between 1.3311 and 2.6 and particle sizes in the range $0.2 - 20 \mu\text{m}$. The inset (b) on the right focuses on the ranges which were most relevant for our work: refractive indices between 1.3311 and 1.6500 and particle sizes ranging from 0.2 to $10 \mu\text{m}$. Both images are normalized to their peak value. (c) C_{ext} vs d for different refractive indices as retrieved from the LUT. Oscillations in Mie functions leading to a non-monotonic behavior occur at smaller diameters for increasing n .

For any given n , a size is associated through the LUT to each C_{ext} bin, hence the corresponding histogram value. The LUT has been calculated over a size range of $0.2 - 20 \mu\text{m}$ and a refractive

index range of $1.3311 - 2.6$. The minimum value of n is determined by that of pure water at the operative wavelength of 670 nm ($n_{H_2O} = 1.3310$). In Figure 2.11, the algorithm working procedure is shown for hypothetical samples with $n = 1.42$, $n = 1.46$ and $n = 1.56$, all of them characterized by a Gaussian PSD with average $4.5 \mu\text{m}$ and variance $0.3 \mu\text{m}$ (black and white histograms). Red histograms are the hypothetical results of measurements providing the PSD obtained through LO. DEDALO allows to recover the effective Gaussian histograms from them. The red dashed line represents the calibration curve, adopted here to convert d into C_{ext} . The black solid curves are obtained from the LUT for the considered refractive index, to convert C_{ext} into d . As discussed in more detail below, the remarkable difference between the distributions proves the need to consider the true refractive index to avoid systematic errors in the PSDs. Following the manufacturer's indications, the instrumental calibration curve should be characterized periodically and each time the instrument is subject to relevant changes that could affect the results.

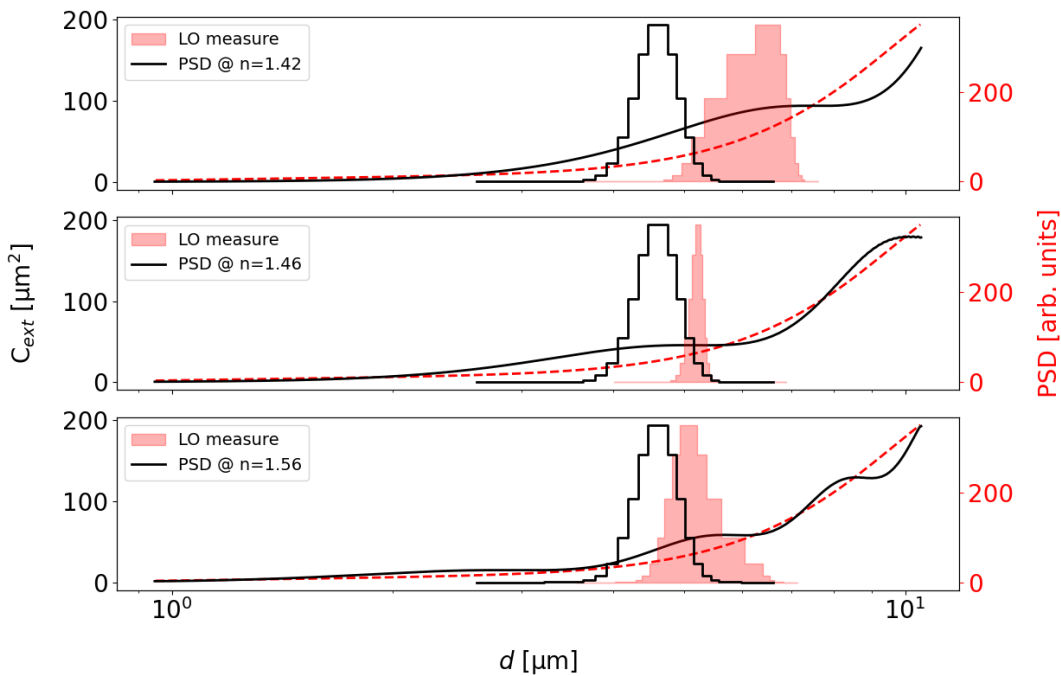


Figure 2.11: Example of the PSD conversion process. Black solid lines represent the C_{ext} curves for $n = 1.42$, $n = 1.46$ and $n = 1.56$ respectively, according to Mie theory. The red dashed curve is the LO calibration function. The red histograms are the result of unprocessed LO measurements, whereas the black and white histograms are the effective initial Gaussian PSDs. DEDALO processes the red histograms to give the correct ones.

DEDALO allows the user to operate the LO instrument in-line, requiring only the value of the flow rate as an input. This is just to calculate particle concentrations based on particle counts. During the measurement, DEDALO shows the instantaneous (1 s integration time) and the time-integrated PSD, as well as the instantaneous numeric concentration of the sample. A continuous monitoring of the working parameters is provided. The instantaneous and time-integrated PSDs are shown in the interface and are written into a file, together with some statistical markers such as the PSD mode diameter and the distribution quantiles. For convenience, the data is copied into a spreadsheet file as well as a plain text file, to comply with most data visualization tools.

2.3.2 The RI correction interactive panel

The analyses described in 2.3.1 are organized in a single interactive window according to the following layout:

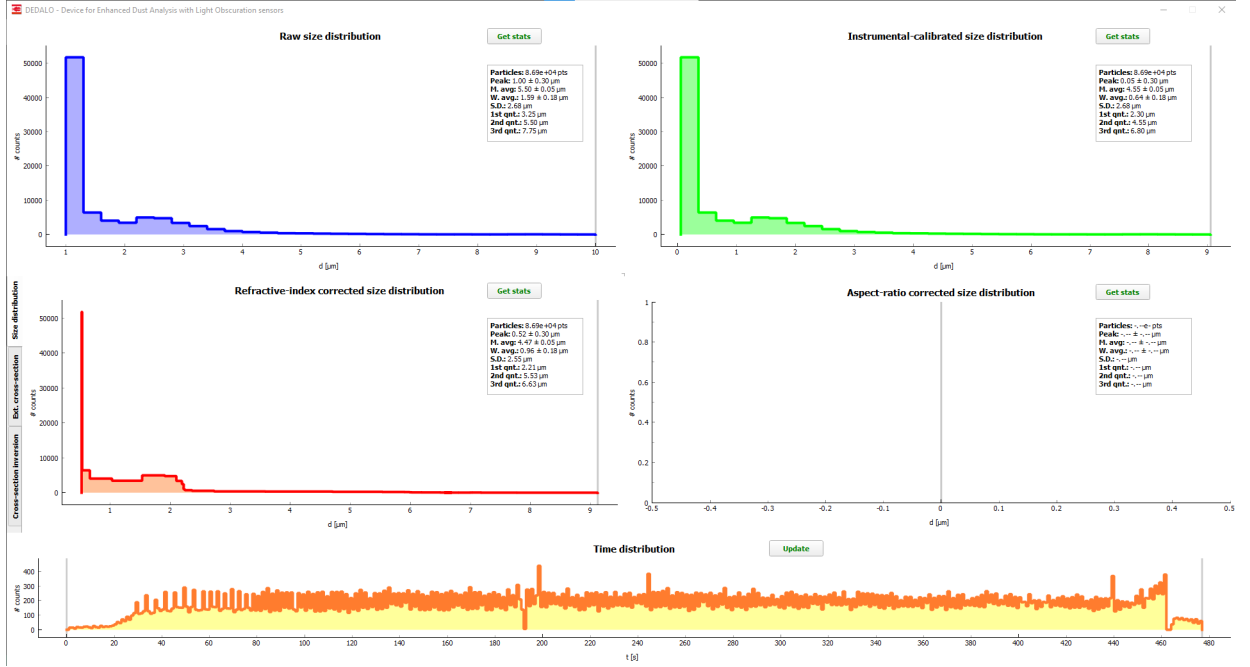


Figure 2.12: Window resuming the different kind of analyses described above. The blue histogram in the upper left corner is the raw uncalibrated size distribution measured by the Abakus laser sensor; the green one, on the right, describes the calibrated size distribution starting from the considerations explained in Section ???. Finally, the red size distribution in the lower left corner is the one obtained after the inversion with the refractive index value(s) set by the user in the appropriate window. Further information on this third procedure are presented in the following. On the bottom, the time distribution of the number of counts is reported as well, so that the user can choose to consider the whole measurement or just a slice of it (limiting consequently the number of particles visualized in the size distributions) by moving the vertical cursors.

In the upper left corner the size distribution is the uncorrected raw one, as measured by the Abakus laser sensor, while on the right side the user can see the calibrated distribution (based on polystyrene extinction measurements). In the lower left corner it is visualized the size distribution after the compensation on the desired refractive index; lastly, the lower right corner is devoted to the aspect-ratio correction which is still work in progress.

The section devoted to the refractive index inversion, as you can see, consists of three separate plots: the first one, immediately displayed when running the software, is precisely the size distribution after this kind of correction; the second one shows a comparison between the extinction cross-section curve for polystyrene perfectly smooth spheres @ 670 nm and the same function evaluated from Mie scattering theory for spherical particles of the selected refractive index. Lastly, the third figure represents the inversion curve used for retrieving the corrected size distribution, that is the particle diameter as a function of the extinction cross-section (red line), and the polynomial fit applied (black line).

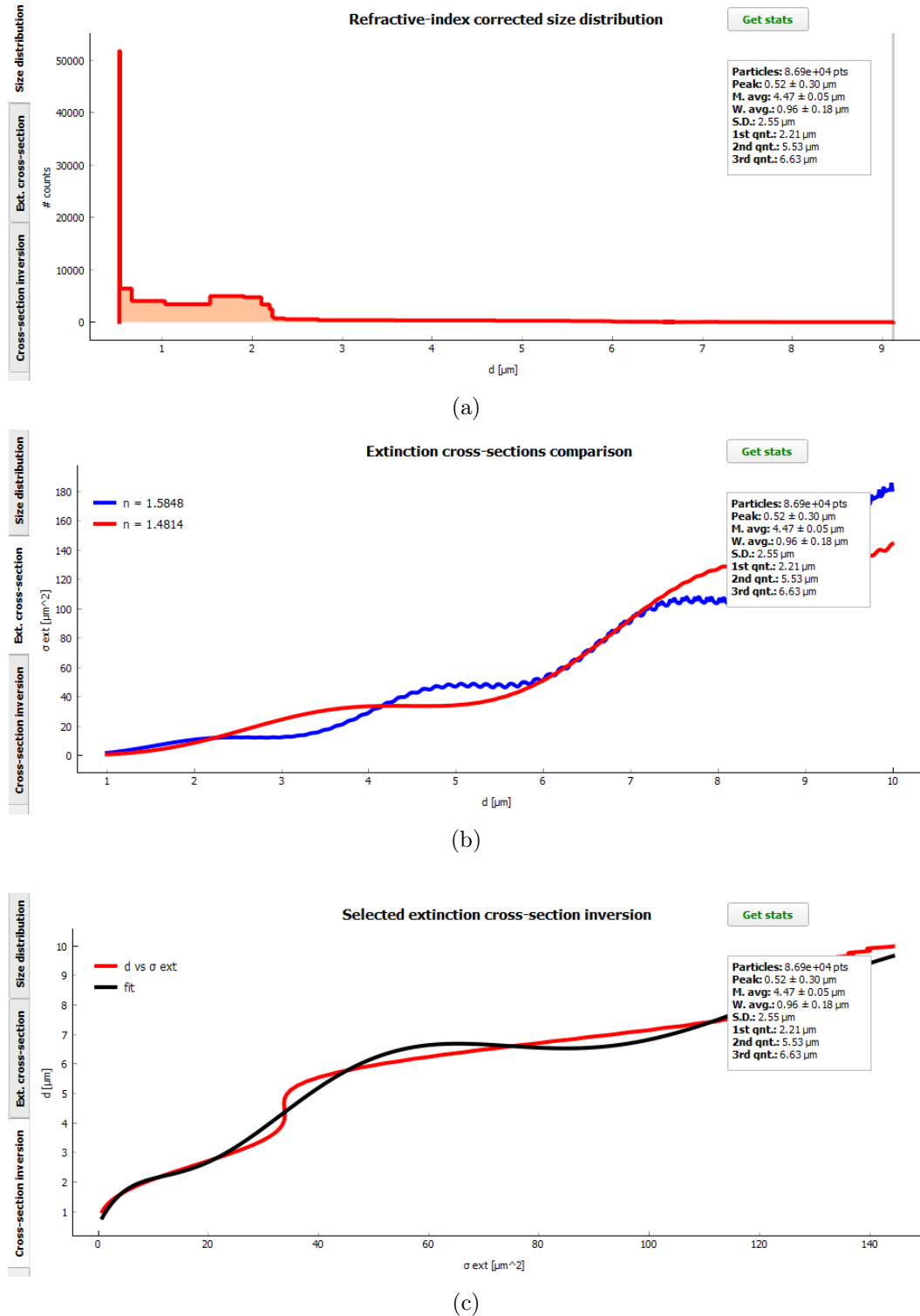


Figure 2.13: .

2.3.3 Aspect-ratio correction

This is the case of non-spherical particles (such as prolate or oblate spheroids, plates or disks), but is STILL WORK IN PROGRESS...

It will be of fundamental importance to implement also this kind of correction since the LO instrument relies on the spherical particles approximation, resulting in obvious alternations of the real particle size distribution of the sample (since mineral dust particles are never spherical in shape).

For more informations on the classes, funtions and methods used to achieve this software, plase have a look at Appendix B.

If you still have some doubts, questions or suggestions for making the software better and nicer, feel free to contact dr. Luca Teruzzi:

- Mail: luca.teruzzi@unimi.it

Chapter 3

Appendix A: Mie theory and light extinction

When a particle is illuminated by a beam of monochromatic radiation, the angular distribution of the scattered light depends strongly on the nature of the particle itself, i.e., its shape and size and the material of which it is composed.

In the following, the Mie scattering problem is addressed in the specific case of particles with spherical geometry, for which there is an exact analytical solution to the scattering problem.

The spherical wave scattered by the particle is modulated by the so-called scattering complement amplitudes $S_1(\theta)$ and $S_2(\theta)$, relative to the two different possible polarizations of the incident wave. They are analytically defined by the expressions [4, 17]

$$\begin{cases} S_1(\theta) = \sum_{n=1}^{+\infty} \frac{2n+1}{n(n+1)} [a_n \pi_n(\cos \theta) + b_n \tau_n(\cos \theta)], \\ S_2(\theta) = \sum_{n=1}^{+\infty} \frac{2n+1}{n(n+1)} [b_n \pi_n(\cos \theta) + a_n \tau_n(\cos \theta)], \end{cases} \quad (3.1)$$

dove θ rappresenta l'angolo di scattering.

The scattering coefficients a_n and b_n that determine the behavior of the spherical wave scattered by the particle are given by the following relations [4, 3]:

$$\begin{cases} a_n = \frac{m\psi_n(mx)\psi'_n(x) - \psi_n(x)\psi'_n(mx)}{m\psi_n(mx)\xi'_n(x) - \xi_n(x)\psi'_n(mx)}, \\ b_n = \frac{\psi_n(mx)\psi'_n(x) - m\psi_n(x)\psi'_n(mx)}{\psi_n(mx)\xi'_n(x) - m\xi_n(x)\psi'_n(mx)}, \end{cases} \quad (3.2)$$

where ψ_n and ξ_n are the Riccati-Bessel functions, ψ' and ξ' the respective derivatives, x defines the so-called size parameter, and m represents the ratio of the refractive index of the particle n_p to the refractive index of the surrounding medium n_{med} :

$$x = ka = \frac{2\pi a}{\lambda}, \quad m = \frac{n_p}{n_{med}}. \quad (3.3)$$

In Eq. 3.1, the scattering angle-dependent terms are expressed as a function of the associated

Legendre polynomials as

$$\begin{cases} \pi_n(\cos \theta) &= \frac{\partial}{\partial(\cos \theta)} P_n(\cos \theta) = \frac{1}{\sin \theta} P_n^1(\cos \theta), \\ \tau_n(\cos \theta) &= \frac{\partial}{\partial \theta} P_n^1(\cos \theta) = \cos \theta \cdot \pi(\cos \theta) - \sin^2 \theta \frac{\partial \pi_n(\cos \theta)}{\partial(\cos \theta)}. \end{cases} \quad (3.4)$$

They are greatly simplified in the case of zero scattering angle $\theta = 0$. Under this condition, the two scattering amplitudes S_1 and S_2 of Eq. 3.1 are equivalent:

$$S(0) = S_1(0) = S_2(0) = \frac{1}{2} \sum_{n=1}^{+\infty} (2n+1) [a_n + b_n]. \quad (3.5)$$

The trend of both the real and imaginary part of $S(0)$ is shown in Fig.(3.1) for an aqueous suspension spherical particles with different refractive indices, as a function of particles diameter.

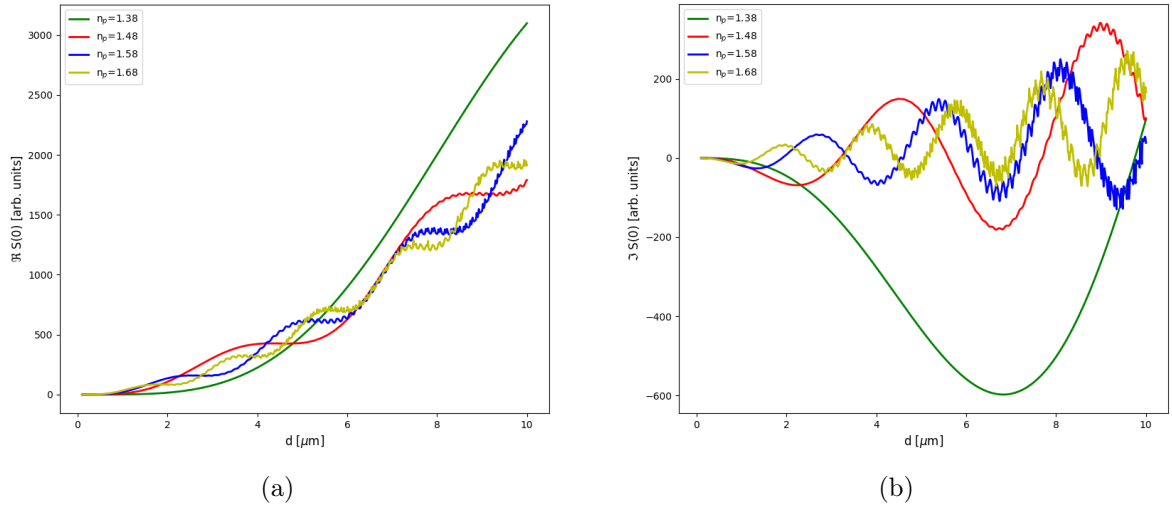


Figure 3.1: Trend of $S(0)$ for an aqueous suspension spherical particles with different refractive indices, as a function of particles diameter between 0.1 and 10 μm .

Moreover, the real part of the complex scattering amplitude is directly linked to the extinction properties of the particle itself: we can define the extinction cross section as [4, 3]

$$C_{ext} = \frac{4\pi}{k^2} \Re\{S(0)\} \quad (3.6)$$

This is the fundamental extinction formula. The extinction process is not a blocking of the incoming wave but a subtle interference phenomenon where the scattered wave removes some of the energy of the original one by interference. The forward scattered wave has an ever weaker influence with increasing z extending over ever wider concentric circles in such a way that the total energy suppressed remains constant and equal to the energy incident on the area C_{ext} .

In Fig.(3.2) are reported the extinction curves corresponding to the values of $\Re\{S(0)\}$ in Fig.(3.1a).

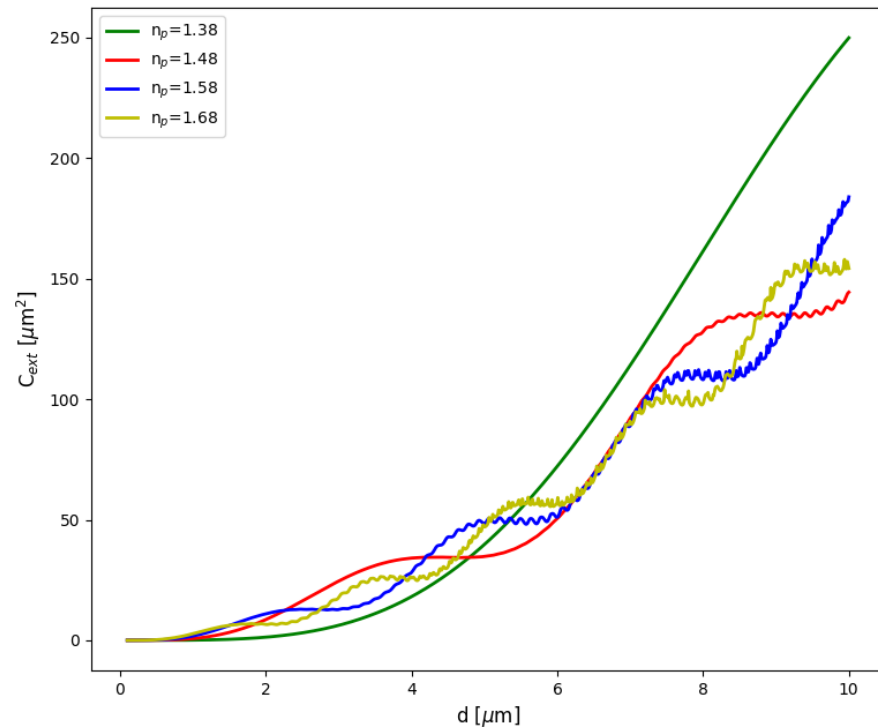


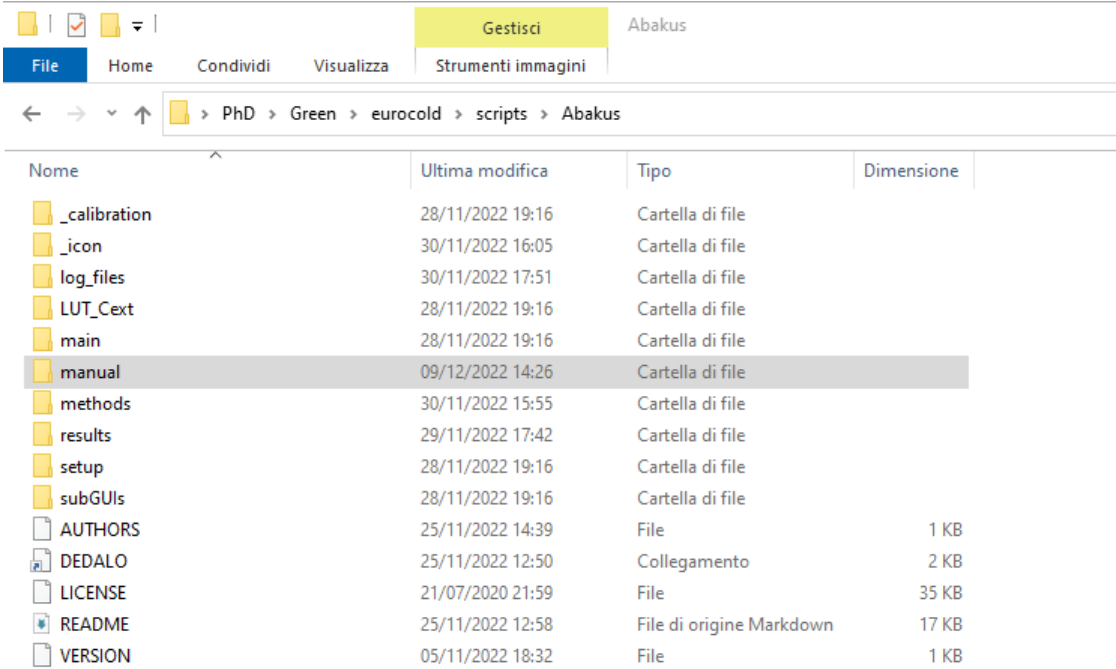
Figure 3.2: Trend of C_{ext} for an aqueous suspension spherical particles with different refractive indices, as a function of particles diameter between 0.1 and 10 μm .

Chapter 4

Appendix B: software back-end examples and requirements

4.1 Folder organization

The software folder is organized as reported in the following picture:



A screenshot of a Windows File Explorer window. The title bar says "Gestisci Abakus". The menu bar includes "File", "Home", "Condividi", "Visualizza", and "Strumenti immagini". The address bar shows the path: "PhD > Green > eurocold > scripts > Abakus". The main area is a table listing files and folders:

Nome	Ultima modifica	Tipo	Dimensione
_calibration	28/11/2022 19:16	Cartella di file	
_icon	30/11/2022 16:05	Cartella di file	
log_files	30/11/2022 17:51	Cartella di file	
LUT_Cext	28/11/2022 19:16	Cartella di file	
main	28/11/2022 19:16	Cartella di file	
manual	09/12/2022 14:26	Cartella di file	
methods	30/11/2022 15:55	Cartella di file	
results	29/11/2022 17:42	Cartella di file	
setup	28/11/2022 19:16	Cartella di file	
subGUIs	28/11/2022 19:16	Cartella di file	
AUTHORS	25/11/2022 14:39	File	1 KB
DEDALO	25/11/2022 12:50	Collegamento	2 KB
LICENSE	21/07/2020 21:59	File	35 KB
README	25/11/2022 12:58	File di origine Markdown	17 KB
VERSION	05/11/2022 18:32	File	1 KB

Figure 4.1: Abakus GUI software repository. The main script is the ‘abakus.pyw’ (the first one), while the others are classes or supplementary modules useful for the software working correctly. Some subfolders are also listed containing text files and GUI configuration files.

In the following the different subfolders are also presented.

- the *subGUIs* folder contains all the .ui files for defining the GUI layout;

Nome	Ultima modifica	Tipo	Dimensione
abakus_GUI.ui	06/12/2022 13:40	File UI	23 KB
data_correction.ui	05/12/2022 11:26	File UI	6 KB
scd_panel.ui	06/12/2022 12:51	File UI	6 KB
serial_monitor.ui	02/12/2022 12:07	File UI	10 KB
volt_panel.ui	06/12/2022 12:51	File UI	6 KB

- the *methods* folder consists of some python scripts which perform different tasks;

Nome	Ultima modifica	Tipo	Dimensione
__pycache__	06/12/2022 15:58	Cartella di file	
abakus_class	05/12/2022 11:34	File di origine Pyt...	33 KB
calibration	02/12/2022 11:22	File di origine Pyt...	8 KB
data_correction	05/12/2022 11:32	File di origine Pyt...	19 KB
error_handling	30/11/2022 17:51	File di origine Pyt...	5 KB
my_widgets	06/12/2022 15:58	File di origine Pyt...	18 KB
plot_correction	06/12/2022 15:57	File di origine Pyt...	41 KB
serial_monitor	02/12/2022 12:30	File di origine Pyt...	9 KB

- in the *main* folder the main DEDALO script is located;
- the *setup* folder contains a text file and a setup.py script for installing all the required python packages;

Nome	Ultima modifica	Tipo	Dimensione
requirements	05/12/2022 11:45	Documento di testo	1 KB
setup	05/12/2022 11:39	File di origine Pyt...	2 KB

- in the *LUT_Cext* folder are stored some LUT (Look-Up Table) files for performing the data refractive index correction;

Nome	Ultima modifica	Tipo	Dimensione
LUT_Cext_l=0.67um_nmed=1.3310_m=[1.0001+0.0010j-1.4275+0.0010j]	31/12/2021 00:53	Documento di testo	40,558 KB
LUT_Cext_l=0.67um_nmed=1.3310_m=[1.0001+0.0100j-1.4275+0.0100j]	31/12/2021 08:13	Documento di testo	40,609 KB
LUT_Cext_l=0.67um_nmed=1.3310_m=[1.0001+0.0500j-1.4275+0.0500j]	31/12/2021 17:15	Documento di testo	40,623 KB
LUT_Cext_l=0.67um_nmed=1.3310_m=[1.0001-1.3524j]	30/12/2021 01:38	Documento di testo	33,336 KB
LUT_Cext_l=0.67um_nmed=1.3310_m=[1.0001-1.5778j]	30/01/2022 14:21	Documento di testo	126,471 KB
LUT_Cext_l=0.67um_nmed=1.3310_m=[1.0001-1.9534j]	07/09/2022 17:34	Documento di testo	210,156 KB

- in the *log_files* folder a report file is saved every time some errors or warnings occur during the DEDALO running;

```

report - Blocco note di Windows
File Modifica Formato Visualizza ?

30-11-2022 17:51:41
Traceback (most recent call last):
  File "C:\Users\lteru\Desktop\PhD\Green\europold\scripts\Abakus\main\abakus.pyw", line 276, in connect_widgets
    self.third_panel.btn_voltage_noise.clicked.connect(self.on_voltage_noise_plot_clicked)
AttributeError: 'Ui' object has no attribute 'on_voltage_noise_plot_clicked'

30-11-2022 17:51:50
Traceback (most recent call last):
  File "C:\Users\lteru\Desktop\PhD\Green\europold\scripts\Abakus\main\abakus.pyw", line 276, in connect_widgets
    self.third_panel.btn_voltage_noise.clicked.connect(self.on_voltage_noise_plot_clicked)
AttributeError: 'Ui' object has no attribute 'on_voltage_noise_plot_clicked'

30-11-2022 17:52:04
Traceback (most recent call last):
  File "C:\Users\lteru\Desktop\PhD\Green\europold\scripts\Abakus\main\abakus.pyw", line 274, in connect_widgets
    self.third_panel.btn_help.clicked.connect(self.on_help_clicked)
AttributeError: 'Ui' object has no attribute 'on_help_clicked'

06-12-2022 13:49:55
Traceback (most recent call last):
  File "C:\Users\lteru\Desktop\PhD\Green\europold\scripts\Abakus\main\abakus.pyw", line 403, in on_serial_clicked
    self.abakus = Abakus(self.first_panel.comboBox_port.currentText())
  File "C:\Users\lteru\Desktop\PhD\Green\europold\scripts\Abakus\methods\abakus_class.py", line 45, in __init__
    self._dev = serial.Serial(port, baudrate, bytesize, parity, stopbits, timeout) # Creation of a Abakus object with the specified serial
  File "C:\Users\lteru\AppData\Local\ Packages\PythonSoftwareFoundation.Python.3.9_qbz5n2kfra8p0\LocalCache\local-packages\Python39\site-packages\serial\super(self, self).__init__(*args, **kwargs)
  File "C:\Users\lteru\AppData\Local\ Packages\PythonSoftwareFoundation.Python.3.9_qbz5n2kfra8p0\LocalCache\local-packages\Python39\site-packages\serial\util\self.open()
  File "C:\Users\lteru\AppData\Local\ Packages\PythonSoftwareFoundation.Python.3.9_qbz5n2kfra8p0\LocalCache\local-packages\Python39\site-packages\serial\serialwin
    raise SerialException("could not open port {!r}: {!r}".format(self.portstr, ctypes.WinError()))
  serial.SerialException: could not open port ''': FileNotFoundError(2, 'Impossibile trovare il percorso specificato.', None, 3)

1 elen

```

- the *manual* folder is the one where you are now;
- the *_icon* folder contains all the icon and pictures that appears int eh GUI;
- the *_calibration* folder stores two text files concerning the instrument calibration function;
- in the *results* folder, lastly, the output files of the DEDALO analyses are saved.

4.2 Required packages and setup

To run the script on his own laptop or PC, the user first need to install the specified Python packages:

- numpy ≥ 1.21 , matplotlib $\geq 3.6.2$ and math (default packages);
- pyserial, for setting the serial communication through the RS232 port between the Abakus particle counter and the PC;
- PyQt5, pyqtgraph, qtwidgets required for the graphical user interface;
- termcolor;
- pandas;
- os-sys $\geq 2.1.4$;
- scipy $\geq 1.9.3$ (optimize, interpolate), needed for computing the instrumental calibration curve;
- miepython, for computations regardig Mie scattering parameters (eg. scattering and extinction cross sections);
- openpyxl, for exporting data in xlsx files.

To do so, after installing Python3 and pip3, you can just copy and paste the following line in the command line:

```
pip3 install numpy≥1.21, matplotlib≥3.6.2, os-sys≥2.1.4, pyserial, PyQt5,  
pyqtgraph, qtwidgets, termcolor, scipy≥1.9.3, miepython, openpyxl,  
pandas
```

Otherwise, you can run the setup.py script in the "setup" folder by typing:

```
python3 setup.py
```


Bibliography

- [1] USP. General Chapters: <788> Particulate Matter in Injections, Pharmacop. Forum **28** (2012), USP32-NF27.
- [2] ISO21501-3 Determination of particle size distribution – Single particle light interaction methods – Light extinction liquid-borne particle counter. Standard No. ISO21501-3, Int Org Standard, Geneva, CH (2019).
- [3] H. C. van de Hulst, *Light Scattering by Small Particles*, Dover Publications Inc., New York (1981).
- [4] C. F. Boren, D. R. Huffman, *Absorption and Light Scattering by Small Particles*, Wiley Science Paperback Series, New York (1998).
- [5] L. L. Wang, P. DeRose and A. K. Gaigalas, Assignment of the number of equivalent reference fluorophores to dyed microspheres, *Journal of Research of National Institute of Standards and Technology* **121** (2016), 264–281.
- [6] E. S. Novik, A. V. Dorenskaya, N. A. Borisova and O. V. Gunar, Subvisible Particulate Matter in Therapeutic Protein Injections, *Pharmaceutical Chemistry Journal* **53** (2019), 353-360.
- [7] S. N. Kasarova, N. G. Sultanova and I. D. Nikolov, Temperature dependence of refractive characteristics of optical plastics, *J. Phys. Conf. Ser.* **253** (2010), 012028.
- [8] A. Moujoud, Z. Saddiki, T. Touam, S.I. Najafi Measurement of the refractive-index variations with temperature of hybrid sol-gel glasses, *Thin Solid Films* **422** (2002), 161–165.
- [9] R. M. Waxler and C. E. Weir, Effect of pressure and temperature on the refractive indices of benzene, carbon tetrachloride, and water *J. Res. Natl. Bur. Stand. A Phys. Chem.* **67A(2)** (1963), 163-171.
- [10] Y. Liu and P. H. Daum, The Effect of Refractive Index on Size Distributions and Light Scattering Coefficients Derived from Optical Particle Counter, *J. Aerosol Sci.*, **31**(8) (2000), 945-957.
- [11] T. Werk, D. B. Volkin and H. C. Mahler, Effect of solution properties on the counting and sizing of subvisible particle standards as measured by light obscuration and digital imaging methods, *Eur. J. Pharm. Sci.* **53** (2014), 95–108.
- [12] D. C. Ripple and P. C. DeRose , Primary determination of particle number concentration with Light Obscuration and dynamic imaging particle counters, *J. Res. Natl. Inst. Stan.* **123** (2018), 1-21.

-
- [13] D. C. Ripple and Z. Hu, *Correcting the relative bias of Light Obscuration and flow imaging particle counters*, *Pharm. Res.* **33** (2016), 653–672.
 - [14] A. R. Quiroz, G. Quèbatte, F. Stump, C. Finkler, J. Huwyler, R. Schmidt, H. C. Mahler, A. V. Koulov, and M. Adler, *Measuring subvisible particles in protein formulations using a modified Light Obscuration sensor with improved detection capabilities*, *Anal. Chem.* **87** (2015), 6119-6124.
 - [15] M. F. Simonsen, L. Cremonesi, G. Baccolo, S. Bosch, B. Delmonte, T. Erhardt, H. A. Kjær, M. A. C. Potenza, A. Svensson and P. Valletlonga, *Particle shape accounts for instrumental discrepancy in ice core dust size distributions*, *Clim. Past* **14** (2018), 601–608.
 - [16] <http://stmichaelshospitalresearch.ca/wp-content/uploads/2015/09/Particle-Size-Analysis-Beckman-Coulter-Multisizer-4-Manual.pdf>
 - [17] S. Wolf, N.V. Voshchinnikov, "Mie scattering by ensembles of particles with very large size parameters", *Computer Physics Communications*, **162**, 113-123 (2004).

